

Volume-limited sample of low-mass red giant stars, the progenitors of hot subdwarf stars

I. Sample selection and binary classification method^{*}

Murat Uzundag^{1,2}, Matías I. Jones², Maja Vučković¹, Joris Vos³, Alexey Bobrick⁴, Claudia Paladini²

¹ Instituto de Física y Astronomía, Universidad de Valparaíso, Gran Bretaña 1111, Playa Ancha, Valparaíso 2360102, Chile
e-mail: murat.uzundag@postgrado.uv.cl

² European Southern Observatory, Alonso de Cordova 3107, Santiago, Chile

³ Astronomical Institute of the Czech Academy of Sciences, CZ-25165, Ondřejov, Czech Republic

⁴ Technion - Israel Institute of Technology, Physics Department, Haifa, Israel 32000

ABSTRACT

Context. The current theory predicts that hot subdwarf binaries are produced from evolved low-mass binaries that have undergone mass transfer and drastic mass loss during either a common envelope phase or a stable Roche lobe overflow while on the red giant branch (RGB).

Aims. We perform a spectroscopic survey to find binary systems that include low-mass red giants near the tip of the RGB, which are predicted to be the direct progenitors of subdwarf B (sdB) stars. We aim to obtain a homogeneous sample to search for the observational evidence of correlations between the key parameters governing the formation of sdB stars and constrain the physics of stable mass transfer.

Methods. Based on data from the *Gaia* mission and several ground-based, multi-band photometry surveys, we compiled a sample of low-mass red giant candidates. The candidates were selected according to their *Gaia* data release 2 (DR2) color, absolute magnitude and proper motion cuts. In this work, we concentrated on the southern hemisphere targets and conducted a spectroscopic survey of 88 red giant stars to search for the long-period RGB + MS binary systems within 200 pc. Combining radial velocity (RV) measurements from ground-based observations with CORALIE and RV measurements from *Gaia* DR2 and early data release 3 (eDR3) as well as the astrometric excess noise and RUWE measurements from *Gaia* DR3, we defined a robust binary classification method. In addition, we searched for known binary systems in the literature and in the *Gaia* DR3.

Results. We select a total of 211 RGB candidates in the southern hemisphere within 200 pc based on the *Gaia* DR2 color-magnitude diagram. Among them, a total of 33 red giants were reported as binary systems with orbital periods between 100 and 900 days, some of which are expected to be the direct progenitors of wide binary sdB stars. In addition, we classified 37 new MS + RGB binary candidates, whose orbital parameters will be measured with future spectroscopic follow-up.

Conclusions. Using high-quality astrometric measurements provided by the *Gaia* mission coupled with high-resolution spectroscopy from the ground, we provide a powerful method to search for low-mass red giant stars in long-period binary systems.

Key words. stars:low-mass – stars: subdwarfs – stars: late-type - binaries: spectroscopic - catalogs

1. Introduction

Hot subdwarf B stars (sdBs) are evolved low-mass red giants that have had almost all of their envelope stripped away near the tip of the first red giant branch (RGB), according to standard evolutionary scenarios (Dorman & Rood 1993). They are evolved, compact ($\log g = 4.5 - 6.5$ dex) and hot ($T_{\text{eff}} = 20\,000 - 40\,000$ K) objects with radii between $0.15 R_{\odot}$ and $0.35 R_{\odot}$, located on the so-called extreme horizontal branch (EHB; see Heber 2016, for a review). Their characteristic mass is close to the core-He-flash mass ($\sim 0.47 M_{\odot}$) and they have a very thin hydrogen envelope ($M_{\text{H}} < 0.01 M_{\odot}$). It was found that a large proportion of sdBs (40–70%) are in binaries (e.g. Maxted et al. 2001; Napiwotzki

et al. 2004; Copperwheat et al. 2011), implying that binary interactions are the most likely explanation for their formation.

The three binary formation channels that contribute to the sdB population are: the common-envelope (CE) ejection channel (Paczynski 1976; Han et al. 2002), the stable Roche-lobe overflow (RLOF) channel (Han et al. 2002, 2003) and a binary white-dwarf (WD) merger (Webbink 1984). The sdB component in both binary scenarios (CE and RLOF) has a relatively narrow mass range, peaking at $0.47 M_{\odot}$, whereas the double helium WD merger channel creates a single subdwarf star with a relatively wide and flat distribution, from 0.42 up to $0.72 M_{\odot}$ (Han et al. 2003). Han et al. (2002) showed that the CE ejection channel leads to close binaries with WD or main sequence (MS) companions with short orbital periods ranging from hours to tens of days. Much of the observational research has focused on these short-period systems, and currently, more than 300 short-period sdB systems have been detected (Kupfer et al. 2015; Schaffenroth et al. 2019; Dai et al. 2022, references therein).

^{*} Based on observations collected with the CORALIE echelle spectrograph on the 1.2-m Euler Swiss telescope at La Silla Observatory, European Southern Observatory (ESO) through the Chilean Telescope Time under program ID's CN2019-58, CN2020B-77, CN2022A-82.

The RLOF channel generates sdB+MS binaries with orbital periods ranging from 400 up to 1600 days based on the binary population synthesis models (see red dashed line in Fig. 3 of Vos et al. 2019). These systems are challenging to detect, given their long orbital periods. Long-term observational campaigns have been dedicated to discover these systems over the last decades. Recently, the orbital parameters of long-period sdB binaries have been found for 26 systems (Vos et al. 2019; Otani et al. 2022; Németh et al. 2021; Molina et al. 2022) with periods ranging from 400 to 1600 days. Because both stars are visible in the spectrum, these systems are referred to as "composite" binaries which account for 30–40% of all sdBs (Vos et al. 2019). The observed composite binary systems present correlations between orbital elements, which revealed an invaluable source of information to test the RLOF channel. One of the first correlations that have been found is that between eccentricity and period in which the eccentricity increases with increasing orbital period (Vos et al. 2015). This finding contradicts evolutionary models since all current models predict circular orbits. Vos et al. (2015) demonstrated that the observed eccentricities of wide sdB binaries may be explained by combining two eccentricity pumping mechanisms, phase-dependent RLOF and a circumbinary disk. These models, on the other hand, fail to replicate the observed trend of greater eccentricity with longer orbital periods. Furthermore, the wide sdB binaries show another correlation between the mass ratio (q) and the orbital period (P_{orb}) (Vos et al. 2019). The chemical history of our Galaxy can precisely explain the observed relationship between the mass ratio and the orbital period in long-period sdB binaries as found by Vos et al. (2020). The authors performed a small but statistically significant binary population synthesis study with the binary stellar evolution code MESA considering binaries with primary masses between $0.7 M_{\odot}$ and $2.0 M_{\odot}$ and initial periods between ~ 100 and ~ 900 days. The authors find three important correlations between the properties of the sdB + MS binaries and their progenitors. The RG mass is inversely correlated with the mass ratio of the sdB + MS system, the RG + MS orbital period is correlated with the sdB + MS mass ratio, and lastly the metallicity is correlated with the MS mass in the sdB + MS systems. They also provide ranges on the orbital periods and mass ratios of RG + MS systems that can form wide sdB binaries. By studying the properties of the RG + MS binaries, we can verify if the population of RG + MS binaries matches the requirements needed to produce the observed number of wide sdB binaries. Furthermore, since several properties are linked directly between the progenitors and the final sdB binaries, knowing the distribution of those parameters in the RG + MS binaries will directly predict the expected observed population, and will allow for a strict test of the proposed formation channel.

The aim of this study is to analyze the observed characteristics of a statistically significant volume-limited sample of low mass evolved RGB binaries that are potential progenitors of the wide sdB binaries. We perform a spectroscopic survey searching for binarity among selected low-mass RGB candidates. In future, obtained orbital solutions of RGB+MS binaries initiated by this work will be quite useful for comparing the population of progenitors with the population of the long-period sdB binaries. The observed volume-limited sample composed of pre- and post-mass transfer binaries will provide additional information about the details of mass transfer in these systems, as well as the nature of the period-eccentricity relation observed in long-period systems.

The paper is organized as follows. In Section 2, we provide the sample selection from *Gaia* DR2 and the literature. In Sect.

3, we describe the EULER/CORALIE observations and data reduction. In Sect. 4, we describe our classification method to search for low-mass red giants in long-period binary systems. Finally, in Sect. 5, we summarize our results and give an outlook for the future.

2. Target selection

To select the low-mass red giant candidates, we have used the *Gaia* mission data release 2 catalog (DR2; Gaia Collaboration et al. 2018) in combination with synthetic colors for RG stars obtained from the MESA Isochrones and Stellar Tracks (MIST; Choi et al. 2016). First, we applied the criteria on photometric and astrometric quality as described in Lindegren et al. (2018, Appendix C). Then, we chose objects in the region defined by the four functions below:

$$G_{\text{abs}} = 2.19(G_{BP} - G_{RP}) - 1.95; \quad (1)$$

$$G_{\text{abs}} = 1.86(G_{BP} - G_{RP}) - 1.10; \quad (2)$$

$$G_{\text{abs}} = 45(G_{BP} - G_{RP}) - 43.9; \quad (3)$$

$$G_{\text{abs}} = 28.33(G_{BP} - G_{RP}) - 38.28; \quad (4)$$

where G_{abs} is an absolute *Gaia* G magnitude. Since phot_g_mean_mag of *Gaia* is apparent magnitude, $G_{\text{abs}} = \text{phot_g_mean_mag} + 5 \log_{10}(\text{parallax}/1000) + 5$. These cuts focus on the systems prior to the tip of the RGB, and cut off evolved higher-mass systems. Equations 1 and 4 provided the cuts to exclude the contaminants from the subgiant and horizontal branch stars, while equations 2 and 3 provided the cuts to remove the contaminants from the red clump stars. The selected region is shown in Fig. 1 (left panel) as a red shaded region, which includes a total of 6158 targets. We did an external cross-match with several catalogues using TOPCAT (Taylor 2005). The literature was searched through the SIMBAD Astronomical Database¹ (Wenger et al. 2000) and we removed 158 outlier objects which turn out to be various types of systems from long period variables (LP) to neutron stars (N^*). The remaining 6000 targets were then cross-matched with the other large-area surveys using a 5 arcsec aperture in order to clean the sample further. We cross-matched the data with the GALEX DR5 All-sky Imaging Survey (AIS; Bianchi et al. 2011) and found 3331 objects with NUV and FUV measurements. In order to obtain the near-IR measurements, we cross-matched these objects with the Wide-field Infrared Survey Explorer (WISE; Wright et al. 2010), and found 3325 targets with their W1 and W2 band measurements. Likewise, the other IR surveys, including Infrared Astronomical Satellite (IRAS; Neugebauer et al. 1984) and the Infrared Astronomical Mission (AKARI; Murakami et al. 2007) were cross-matched to exclude the targets further if they show any excess. The UV excess indicates WD companions while the IR-excess indicates the presence of disks or dust. These kinds of systems (548 stars) were excluded from the survey since we are searching for RG + MS stars that have not yet undergone any type of binary interaction. Finally, we selected 2777 low-mass RG candidates within 500 pc covering the southern and northern

¹ <https://simbad.u-strasbg.fr/>

hemispheres. All selected objects have an error on the parallax lower than 10 %.

In this study, we limited ourselves only to the southern hemisphere ($\delta \leq 20^\circ$) and to the smaller volume of 200 pc so that we have a feasible number of systems for a pilot study. Within 200 pc, we have a total of 211 low-mass RG candidates in the southern hemisphere. In Fig. 1, we present the color-magnitude diagram of selected low-mass RG candidates within 200 pc with blue dots (left panel) and their spatial distribution with respect to the galactic coordinate system (right panel).

2.1. Spectroscopic binaries from the literature

We searched for known low-mass RGs from the literature applying the similar selection criteria as described in Sect. 2. We found a total of 300 binaries detected by different spectroscopic surveys (e.g. Setiawan et al. 2004; Jones et al. 2011; Massarotti et al. 2008; Wittenmyer et al. 2011). Among them, we identified 24 RG binary systems with orbital periods ranging from 100 to 900 days, which could be potential progenitors of wide sdB + MS composite systems produced by RLOF mechanism. The orbital elements of these systems are listed in Table 1 including the orbital period of the binary system (P), the amplitude of the radial velocity curve (K), the eccentricity of the orbit (e), angle of periastron (ω), time of periastron (T_0) and the mass function ($f(m)$).

2.2. Binaries from DR3

We made use of Non-single stars catalog (I/357²) from *Gaia* DR3 (Gaia Collaboration et al. 2022) to detect more binary stars within 200 pc. To select all RG candidates in binary systems, we used the same selection criteria described in Sect. 2. DR3 catalog includes astrometric, spectroscopic, and eclipsing binaries (where solutions from the combinations of astrometry and radial velocities, or eclipsing binary light curves and radial velocities are also provided; Gaia Collaboration et al. 2022). From the *Gaia* DR3 catalog, we found nine binary systems with orbital periods between 100 and 900 days. All these systems and their orbital elements are presented in Table 2.

3. Observations and data reduction

3.1. Observations and data reduction using CORALIE

The spectroscopic observations of the low-mass RGB candidates analyzed in this paper were obtained with the CORALIE echelle spectrograph (Queloz et al. 2001) mounted at the Swiss 1.2-metre Leonhard Euler Telescope at La Silla Observatory in Chile. CORALIE has a resolving power of $R \sim 60000$, allowing for a long-term radial velocity precision up to 0.03 km s^{-1} (Queloz et al. 2001). CORALIE is fed by two fibers: a 2'' diameter on-sky science fiber encompassing the star, and another that can either be connected to a Fabry-Pérot etalon for simultaneous wavelength calibration (used in the case of our survey) or on-sky for background subtraction of the sky flux.

From the 200 pc RG sample, we observed 82 stars with Euler/CORALIE. The observations were done in three different runs. The details of these observations are given in Table 3 including the instrument, date, spectral range and the signal-to-noise (S/N) ratio. The observed stars have a photometric G mean magnitude ranging from 5 to 9 with a median of 7.5.

The observed sample is depicted in Fig. 1 (red dots). In total, we obtained 123 high-resolution CORALIE spectra for 82 stars. We reduced and analyzed the data using the customized CERES pipeline (Brahm et al. 2017), which performs all the extraction processes from basic bias, dark and flat-field corrections (including scattered light) to order tracing, wavelength calibration, and computation of precise radial velocities using the cross-correlation technique. For 38 objects, we obtained two epochs spectra and measured their RV shifts. The RV measurements from multi-epoch CORALIE observations are listed in the tables in the Appendix A. The difference between these two different epochs is defined as ΔCRV and is provided in Table 4.

3.2. ESO archival data

We used the ESO archive³ to search for high-resolution spectra of stars in our sample. We found a total of 8 stars observed with HARPS and 19 targets observed with FEROS. However, most of them (18 stars) were observed by the EXPRESS RV program (Jones et al. 2011; Soto et al. 2021), whose spectroscopic binaries were presented in Bluhm et al. (2016) and are listed in Table 1. One star is in a WD+AFGK binary system (Ren et al. 2020) and two objects are found to be single planet-host stars (Yilmaz et al. 2017; Wittenmyer et al. 2020), which are discarded from our analysis. Finally, our analysis includes six stars observed with FEROS. The CERES pipeline was used to reduce the FEROS spectra as it was for CORALIE data.

4. Classification Method

4.1. Astrometric excess noise

The high astrometric precision currently made possible by missions such as *Gaia* provides several important parameters. One of the most important parameters for this work is the *Gaia* DR2 astrometric excess noise (AEN), which is a measure of the residuals in the source's 5-parameter astrometric solution. It can be used in astrometric binary system classification since a higher AEN value might indicate the presence of unresolved companions. Gandhi et al. (2022) reviewed the details and feasibility of this method, as well as an effective way to use AEN to search for X-ray binaries.

For our study, we made use of AEN to search for low mass RG binary candidates in our sample. Starting from the 33 known RG binaries (from the literature and DR3), we analyzed their AEN measurements. Out of 33 known binaries 31 have $\text{AEN} \geq 0.4 \text{ mas}$ (see Fig. 2 filled circles). Given that more than 90% of the known binaries have $\text{AEN} \geq 0.4 \text{ mas}$, we have chosen this value of AEN as a threshold to consider that a star is a potential binary candidate. In other words, these targets will be further followed up in order to confirm the binarity and finally obtain orbital periods.

4.2. The Renormalised Unit Weight Error (RUWE)

The *Gaia* data product known as the Renormalised Unit Weight Error (RUWE) is a measure used to filter out sources with potentially bad astrometry, in particular spurious parallaxes or proper motions (see for details, Lindegren et al. 2018). The RUWE is expected to be around 1.0 for sources where the single-star model provides a good fit to the astrometric observations. If a value is significantly greater than 1.0, that could indicate that

² <https://cdsarc.cds.unistra.fr/viz-bin/cat/I/357>

³ http://archive.eso.org/eso/eso_archive_main.html

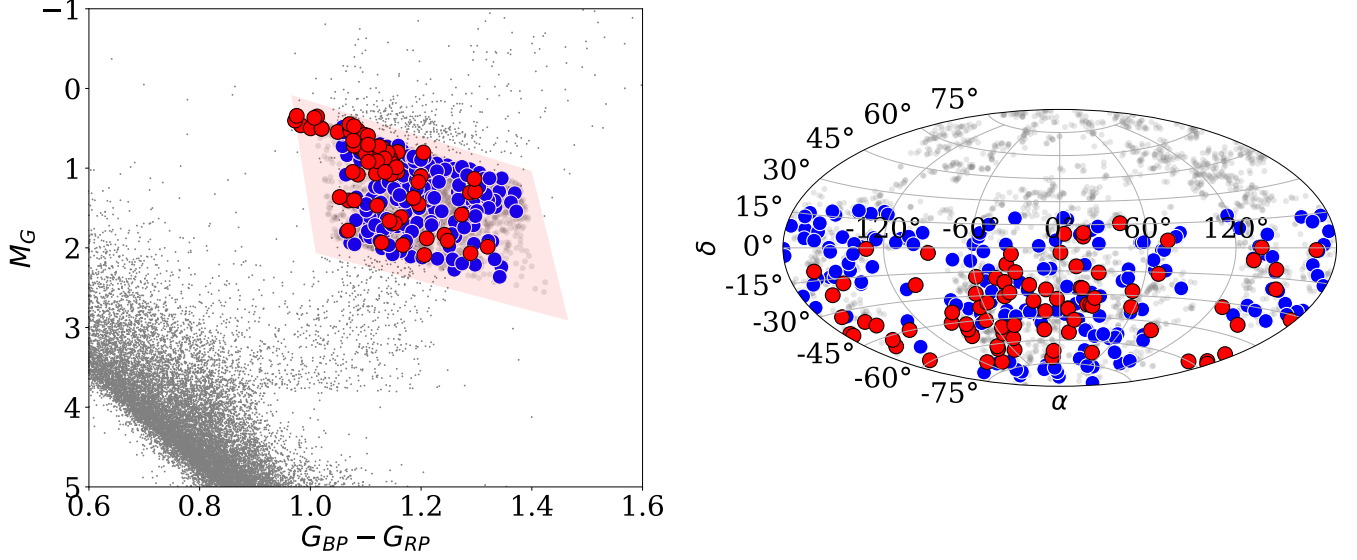


Fig. 1. LEFT: The color-magnitude diagram of all low-mass ($0.7 - 2.3 M_{\odot}$) RG candidates within 200 pc (blue dots) from *Gaia* DR2, including only the southern hemisphere stars. As a comparison, the *Gaia* DR2 color-magnitude diagram of the 100 pc clean sample (Sample C in [Lindgren et al. 2018](#)) is shown in grey. The slightly larger grey dots within the selected sample represent the low-mass RG candidates within 500 pc. The red circles show the low-mass RG candidates that were observed with EULER/CORALIE. RIGHT: Sky locations (Galactic coordinates, Aitoff projection) of the volume-limited low-mass RG sample within 200 pc with respect to the galactic coordinate system using the same color coding.

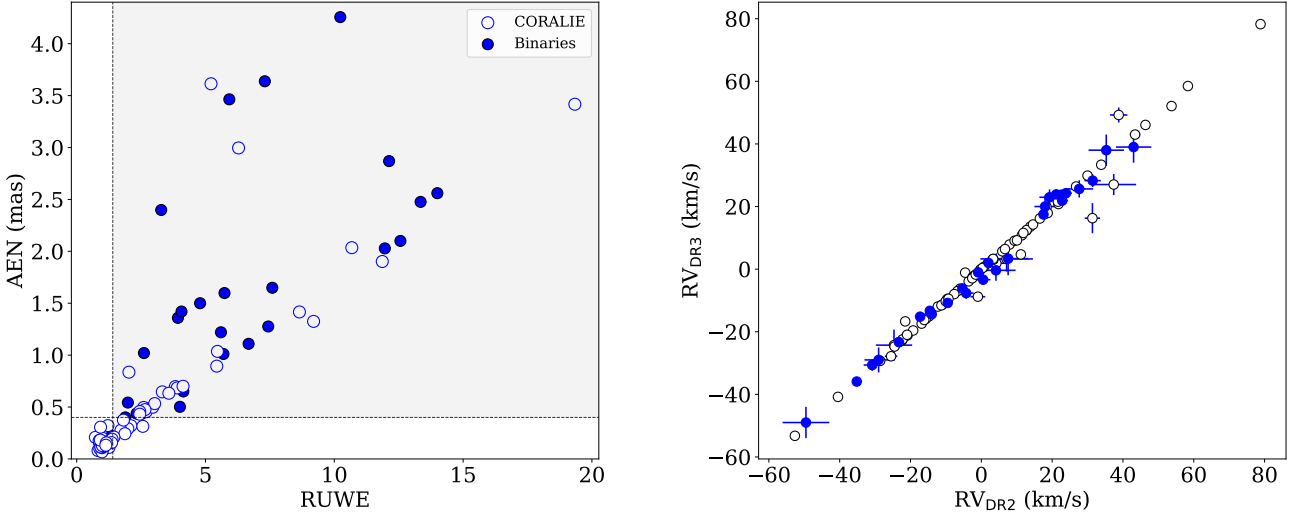


Fig. 2. LEFT: AEN versus RUWE, including known binaries from the literature and DR3 (filled blue circles) and observed stars (open blue circles). AEN of 0.4 mas is represented by the horizontal black dashed line, and RUWE of 1.4 is represented by the vertical black dashed line. The gray-shaded area displays all the stars that are most likely in binary systems. RIGHT: Radial velocity measurements from DR3 (y-axis) as a function of radial velocity measurements from DR2 (x-axis) using the same color coding.

the source is not a single object or otherwise problematic for the astrometric solution. Therefore, we used RUWE to search for low-mass RG binary candidates in our sample. We examined the RUWE measurements of the known RG binaries, and we found that 93% of the known binary systems have RUWE bigger than 1.4. Therefore we used $\text{RUWE} \geq 1.4$ as a threshold to consider the object as a binary candidate.

To put this in a perspective, we have plotted known binary systems as well as observed stars with CORALIE and FEROS in AEN and RUWE parameters space indicating our selection

threshold in Fig. 2. The gray shaded area depicts the systems that are potential binaries based on our selection criteria. As can be seen in Fig. 2, all known binaries fall on the grey shaded area.

4.3. Radial velocities from CORALIE, FEROS, DR2 and DR3

In order to define the binary fraction in our observed sample, we made use of the radial velocity measurements from CORALIE, FEROS, *Gaia* DR2 and DR3. The RV measurements from DR2

Table 1. Orbital solutions for all known binaries, including the Hipparcos catalog number, the orbital period of the binary system (P), the amplitude of the radial velocity curve (K), the eccentricity of the orbit (e), angle of periastron ω , time of periastron (T_0) and the mass function ($f(m)$).

HD	HIP	P (day)	K (km s ⁻¹)	e	ω	T_0	$f(m)$ (M_\odot)	Ref.
5516	4463	115.7 (0.2)	17.91 (0.09)	0.003	103	52662	3.3127	2
5877	4618	211.4 (0.3)	12.94 (0.01)	0.1	40.8 (0.6)	5406.3 (0.3)	0.467	3
14355	10548	429.1 (0.3)	6.9 (0.3)	0.3	5.0 (1.9)	5306.6 (1.5)	12.9 (0.2)	3
15755	11840	629.2 (2.7)	10.67	0.14	294.6	53979	0.077	2
27697	20455	522.1 (1.8)	2.84 (0.3)	0.48			0.0084	1
29923	22055	680.1 (25.9)	6.48	0.1	42	53797	0.0189	2
30197	22176	107.6 (0.1)	8.51 (0.15)	0.03	254.5	49457.5	0.00623	2
32008	23221	898.1 (2.7)	5.2	0.17	155.1	51240	0.01248	2
54563	34608	113.4 (0.1)	20.75 (0.04)	0.4				2
62644	37606	380.6 (0.1)	9.84 (0.7)	0.73			0.12	1
65938	39198	365.4 (0.6)	9.56	0.52	108.1	53826.9	0.0208	2
72184	41935	324.1 (16.5)	3.83	0.15	90	54051	0.00183	2
94386	53259	925 (1)	2.18 (0.01)	0.42	37.8 (0.2)	54582.1 (1.2)		2,4
102928	57791	489.6 (0.9)	12.48 (0.2)	0.22	102.4	53114.4	0.0916	2
104358	58601	281.1 (0.3)	1.83 (0.04)	0.24	146 (7)	54836.8 (4.2)		4
133166	73758	97.1 (0.2)	11.82 (0.01)	0.4	53.4 (0.1)	5304.3 (0.1)	0.271	3
136138	74896	508.7 (1.6)	6.19 (0.12)	0.33	39	53751.8	0.01053	2
153438	83224	173.3 (0.3)	8.74 (0.01)	0.3	85.6 (0.3)	5251.3 (0.1)	0.104	3
153956	83138	900.14 (14)	3.36 (0.16)	0.07	338	52956	0.00352	2
172831	91751	485.3 (0.3)	9.68	0.21				2
179799	94521	856.1 (39.1)	5.99 (0.4)	0.66			0.081	1,2
181391	95066	266.5 (0.1)	29.86	0.83				2
199870	103519	635.1 (0.5)	6.44	0.44				2
221625	116243	94.9 (0.1)	36.21	0.52	315.82	53555.4	1.67	2

References. (1) [Setiawan et al. \(2004\)](#); (2) [Massarotti et al. \(2008\)](#); (3) [Bluhm et al. \(2016\)](#); (4) [Wittenmyer et al. \(2016\)](#)

Table 2. Binary systems that are found in DR3, including the name of star, the methods that have been used (astrometric + spectroscopic, astrometric and astrometric, respectively), the orbital period of the system, time of periastron (T_0) and eccentricity of the orbit.

Star	Solution type	Period (days)	T_0 (days)	e
HD2132	AstroSpectroSB1	773	369.636	0.04
HD8410	AstroSpectroSB1	304	30.240	0.22
HD9525	Orbital	582	46.125	0.16
HD36787	AstroSpectroSB1	257	108.608	0.42
HD116338	OrbitalTargetedSearch	248	-34.041	0.84
HD13423	OrbitalTargetedSearch	899	303.991	0.21
HD162049	OrbitalTargetedSearch	713	-83.897	0.45
HD190574	AstroSpectroSB1	552	-90.773	0.70
HD202470	AstroSpectroSB1	488	241.819	0.52

and DR3 are depicted in Fig. 2 (right panel), where we show known binaries with filled blue circles and observed stars with open blue circles. As can be seen in Fig. 2 (right panel), DR2 and DR3 measurements do not differ.

With CORALIE, we obtained two different epochs of spectra (Δ CRV) for 38 stars, which are reported in Table 4 where we also listed the AEN value and the corresponding uncertainty. If the difference in Δ CRV ≥ 0.1 km s⁻¹, we consider it as a potential binary candidate. Out of these 38 observed objects, we found 17

Table 3. Observing log of the spectroscopic data obtained for the low-mass red giant stars studied in this work.

Instrument	Date	Range (Å)	S/N
CORALIE	15-16-17 June 2019	3800-6800	30-80
CORALIE	18-19-20 November 2021	3800-6800	50-100
CORALIE	4 April 2022	3800-6800	40-60

stars that show Δ CRV above the threshold and, therefore, could be potential binary systems.

We obtained a single epoch CORALIE spectrum for 44 stars, which were combined with RV measurements from *Gaia* DR2 in order to measure RV differences. Likewise, a single epoch archival FEROS spectra for 6 stars were combined with RV measurements from *Gaia* DR2. In Table 5, we show the difference between the CORALIE/FEROS RV and the DR2 RV measurements (Δ RV) of all the single epoch observed stars from the ground together with their AEN and RUWE. Given that the errors in *Gaia* DR2 measurements vary from 0.2 to 2.5 km s⁻¹, we have chosen to use the 3σ criteria as the threshold. In other words, if the RV difference between ground base and DR2 RV measurements is three times greater than its RV error, we consider the object as a potential binary candidate.

4.4. Classification

By combining three sets of measurements, AEN, RUWE and RV measurements, we defined three categories that classify a star by its likelihood to be a binary candidate. The stars that have been observed from the ground are divided into three categories. The stars that have at least two of the parameters (AEN/RUWE and RV variation) larger than the threshold we classify as binary candidates and assign them a category 1. The stars that have one of the parameters above the threshold (AEN, RUWE or RV variation) we assign them category 2 as they are likely to be binary candidates. The third group (category 3) includes targets with no significant AEN, RUWE or large RV variations.

In the observed set, we found that 24 stars show $AEN \geq 0.4$, out of which 18 stars also present significant radial velocity variations. It is these 18 stars that we assigned a category 1 as they are binary candidates which will be priority targets for follow-up observations. Furthermore, we found 18 stars that are potential binary candidates (category 2) out of which 13 targets show only significant RV variations, and 5 stars show solely astrometric excess noise above the threshold of 0.4 mas. These 18 stars are also added to the follow-up observations as additional observations are needed to confirm their binarity.

Furthermore, three stars (HD119483, HD149649 and CD-397574) that were observed with CORALIE in two epochs show RV variations of 0.061, 0.046 and -0.046 km s^{-1} , respectively. As these variations are just below the RV threshold of 0.1 km s^{-1} we marked these stars as potential follow-up candidates. Moreover there is one target, HD120144, that has RUWE of 1.37, while it does not show either AEN or RV variation. We consider this target as a possible binary candidate (category 2), which should also be observed in the future.

Lastly, using the same classification method, we classified 6 FEROS targets that were obtained from the ESO archive. One of them corresponds to a binary system listed in the *Gaia* DR3 catalogue, and one more was classified in category 1, i.e., it is most likely a binary candidate.

5. Conclusion and future prospects

Based on the *Gaia* DR2 color-magnitude diagram, we select a sample of 211 low-mass RG candidates within 200 pc in order to search for low-mass RGB + MS binary systems with orbital periods between 100 and 900 days, which are potential progenitors of wide binary sdB systems. From the literature, we found 24 such systems. Furthermore, nine long-period (248 to 898 days) binary systems were identified with orbital parameters from DR3. In addition, we obtained CORALIE spectroscopic data for 82 stars and single-epoch FEROS archive spectra for 6 stars among this sample. We combined the resulting CORALIE and FEROS RVs with the DR2 and DR3 radial velocity measurements, as well as AEN and RUWE values, to search for potential binary candidates. From these combined datasets we defined three different categories based on their likelihood of being a binary candidate. The first group includes binary candidates since they have a large RV variation and a high AEN. The second group contains likely binary candidates since they show either high RV or have AEN values above the threshold. The third group includes the stars that do show neither RV nor AEN variations, which accounts for 53% of the observed sample, or 47 stars. The observed sample demonstrates that 47% of the observed stars (41 out of 88) most likely have binary signatures. This result is not unexpected considering that about half

Table 4. Binary classification of low-mass red giant stars reported in this paper with two CORALIE epochs spectra, including the name of the observed star, the astrometric excess noise (AEN) measurements from *Gaia* eDR3, the difference between two CORALIE RV measurements (ΔCRV), the errors on RV and the classification number.

Star	ΔCRV (km s^{-1})	eRV (km s^{-1})	AEN (mas)	RUWE	Category
HD112521	3.715	0.04	0.68	3.899	1
HD167936	-16.23	0.05	1.42	8.646	1
HD305357	4.276	0.1	0.46	2.447	1
HD214941	3.44	0.06	0.43	2.446	1
HD217614	-10.76	0.05	2.04	10.68	1
HD201013	-5.57	0.04	0.7	4.128	1
HD206005	-0.49	0.03	0.37	1.814	1
HD71464	22.710	0.04	0.15	1.285	2
HD116338	1.358	0.03	0.21	1.445	2
HD136350	-9.882	0.05	0.09	0.998	2
HD139137	0.955	0.06	0.31	2.567	2
HD204381	-0.012	0.04	0.84	2.027	2
HD85885	-0.198	0.04	0.24	1.872	2
HD102805	0.518	0.04	0.09	0.924	2
HD170105	1.067	0.04	0.1	0.897	2
HD157527	-0.306	0.04	0.21	0.724	2
HD99891	-0.136	0.04	0.17	1.352	2
HD120144	0.013	0.04	0.19	1.373	2
HD119483	0.061	0.04	0.15	1.207	3
HD149649	0.046	0.04	0.11	0.954	3
CD-397574	-0.046	0.05	0.08	0.984	3
CD-324787	-0.033	0.05	0.09	0.981	3
HD102216	-0.030	0.04	0.09	1.027	3
HD107045	-0.002	0.04	0.12	0.975	3
HD114430	0.003	0.04	0.12	0.966	3
HD116845	-0.007	0.04	0.1	0.924	3
HD122568	-0.018	0.04	0.11	1.253	3
HD124461	-0.008	0.04	0.14	1.097	3
HD162157	0.001	0.04	0.11	0.966	3
HD167768	0.001	0.05	0.18	0.872	3
HD168839	-0.022	0.04	0.08	0.828	3
HD171864	-0.015	0.04	0.13	1.041	3
HD176771	0.030	0.04	0.16	1.003	3
HD191716	-0.007	0.04	0.12	1.02	3
HD96627	-0.010	0.04	0.16	1.259	3
HD99783	-0.007	0.04	0.12	0.959	3
HD116948	0.013	0.04	0.11	-	3
HD162984	-0.035	0.04	0.11	0.945	3

of low-mass main sequence stars are found in binary systems (Raghavan et al. 2010).

In future work, we will continue observing the selected binary candidates to confirm their binarity and constrain their orbital parameters. Furthermore, the spectra that we obtained will be used to derive accurate atmospheric parameters, including the effective temperature, surface gravity, rotational velocity, micro-turbulence and metallicity. Also, we will derive accurate radii and masses by deriving the radius from an SED fit for the stars that are presented in this work. We note that our sample might suffer from possible contamination from the red clump (RC)

stars, and this contamination can be up to 30% as shown by Girardi (2016). Removing this contamination to define the low-mass RG stars is not easy since they cannot be distinguished by either color-magnitude diagrams or spectroscopic surveys (e.g. Masseron & Hawkins 2017). The way to distinguish these two groups is to use asteroseismology. For instance, Bedding et al. (2011) showed that the seismic parameter called period spacings can be used to distinguish RGB stars, burning only hydrogen in the shell, from RC stars that also burn helium in their cores. In the future, we will make use of this advanced technique using high-precision photometry for the targets that have been observed during TESS and K2 missions. There are several ongoing large-scale, ground-based surveys focused on obtaining high-resolution spectroscopy, including GALAH ($12 \leq V \leq 14$), SDSS V ($11 \leq H \leq 14$) and *Gaia*-ESO (variable brightness ranges). These surveys will be important to constrain the orbital parameters of promising targets that are classified as 1 and 2 in this work.

Acknowledgements. M.U. acknowledges financial support from CONICYT Doctorado Nacional in the form of grant number No: 21190886 and ESO studentship program. M.V. acknowledges support from the grant FONDECYT REGULAR No: 1211941. J.V. acknowledges support from the Grant Agency of the Czech Republic (GAČR 22-34467S). The Astronomical Institute Ondřejov is supported by the project RVO:67985815. A.B. acknowledges support for this project from the European Union's Horizon 2020 research and innovation program under grant agreement No. 865932-ERC-SNeX. Based on observations collected with the CORALIE echelle spectrograph on the 1.2-m Euler Swiss telescope at La Silla Observatory under the program allocated by the Chilean Time Allocation Committee (CNTAC), no: CN2019A-58, CN2019B-87, CN2020B-77, CN2022A-82. This work has made use of data from the European Space Agency (ESA) mission *Gaia* (<https://www.cosmos.esa.int/Gaia>), processed by the *Gaia* Data Processing and Analysis Consortium (DPAC, <https://www.cosmos.esa.int/web/Gaia/dpac/consortium>). Funding for the DPAC has been provided by national institutions, in particular the institutions participating in the *Gaia* Multilateral Agreement.

References

- Bedding, T. R., Mosser, B., Huber, D., et al. 2011, *Nature*, 471, 608
 Bianchi, L., Herald, J., Efremova, B., et al. 2011, *Ap&SS*, 335, 161
 Bluhm, P., Jones, M. I., Vanzì, L., et al. 2016, *A&A*, 593, A133
 Brahm, R., Jordán, A., & Espinoza, N. 2017, *PASP*, 129, 034002
 Choi, J., Dotter, A., Conroy, C., et al. 2016, *ApJ*, 823, 102
 Copperwheat, C. M., Morales-Rueda, L., Marsh, T. R., Maxted, P. F. L., & Heber, U. 2011, *MNRAS*, 415, 1381
 Dai, M., Chen, X., Wang, K., et al. 2022, arXiv e-prints, arXiv:2201.03721
 Dorman, B. & Rood, R. T. 1993, *ApJ*, 409, 387
 Gaia Collaboration, Babusiaux, C., van Leeuwen, F., et al. 2018, *A&A*, 616, A10
 Gaia Collaboration, Creevey, O. L., Sarro, L. M., et al. 2022, arXiv e-prints, arXiv:2206.05870
 Gandhi, P., Buckley, D. A. H., Charles, P. A., et al. 2022, *MNRAS*, 510, 3885
 Girardi, L. 2016, *ARA&A*, 54, 95
 Han, Z., Podsiadlowski, P., Maxted, P. F. L., & Marsh, T. R. 2003, *MNRAS*, 341, 669
 Han, Z., Podsiadlowski, P., Maxted, P. F. L., Marsh, T. R., & Ivanova, N. 2002, *MNRAS*, 336, 449
 Heber, U. 2016, *PASP*, 128, 082001
 Jones, M. I., Jenkins, J. S., Rojo, P., & Melo, C. H. F. 2011, *A&A*, 536, A71
 Kupfer, T., Geier, S., Heber, U., et al. 2015, *A&A*, 576, A44
 Lindgren, L., Hernández, J., Bombrun, A., et al. 2018, *A&A*, 616, A2
 Massarotti, A., Latham, D. W., Stefanik, R. P., & Fogel, J. 2008, *AJ*, 135, 209
 Masseron, T. & Hawkins, K. 2017, *A&A*, 597, L3
 Maxted, P. F. L., Heber, U., Marsh, T. R., & North, R. C. 2001, *MNRAS*, 326, 1391
 Molina, F., Vos, J., Németh, P., et al. 2022, *A&A*, 658, A122
 Murakami, H., Baba, H., Barthel, P., et al. 2007, *PASJ*, 59, S369
 Napiwotzki, R., Karl, C. A., Lisker, T., et al. 2004, *Ap&SS*, 291, 321
 Németh, P., Vos, J., Molina, F., & Bastian, A. 2021, *A&A*, 653, A3
 Neugebauer, G., Habing, H. J., van Duinen, R., et al. 1984, *ApJ*, 278, L1
 Otani, T., Lynas-Gray, A. E., Kilkeny, D., et al. 2022, *ApJ*, 926, 17
 Paczynski, B. 1976, in *Structure and Evolution of Close Binary Systems*, ed. P. Eggleton, S. Mitton, & J. Whelan, Vol. 73, 75

- Queloz, D., Mayor, M., Udry, S., et al. 2001, *The Messenger*, 105, 1
 Raghavan, D., McAlister, H. A., Henry, T. J., et al. 2010, *ApJS*, 190, 1
 Ren, J. J., Raddi, R., Rebassa-Mansergas, A., et al. 2020, *ApJ*, 905, 38
 Schaffenroth, V., Barlow, B. N., Geier, S., et al. 2019, *A&A*, 630, A80
 Setiawan, J., Pasquini, L., da Silva, L., et al. 2004, *A&A*, 421, 241
 Soto, M. G., Jones, M. I., & Jenkins, J. S. 2021, *A&A*, 647, A157
 Taylor, M. B. 2005, in *Astronomical Society of the Pacific Conference Series*, Vol. 347, *Astronomical Data Analysis Software and Systems XIV*, ed. P. Shopbell, M. Britton, & R. Ebert, 29
 Vos, J., Bobrick, A., & Vučković, M. 2020, *A&A*, 641, A163
 Vos, J., Østensen, R. H., Marchant, P., & Van Winckel, H. 2015, *A&A*, 579, A49
 Vos, J., Vučković, M., Chen, X., et al. 2019, *MNRAS*, 482, 4592
 Webbink, R. F. 1984, *ApJ*, 277, 355
 Wenger, M., Ochsenbein, F., Egret, D., et al. 2000, *A&AS*, 143, 9
 Wittenmyer, R. A., Butler, R. P., Horner, J., et al. 2020, *MNRAS*, 491, 5248
 Wittenmyer, R. A., Endl, M., Wang, L., et al. 2011, *ApJ*, 743, 184
 Wittenmyer, R. A., Liu, F., Wang, L., et al. 2016, *AJ*, 152, 19
 Wright, E. L., Eisenhardt, P. R. M., Mainzer, A. K., et al. 2010, *AJ*, 140, 1868
 Yilmaz, M., Sato, B., Bikmaev, I., et al. 2017, *A&A*, 608, A14

Table 5. Binary classification of low-mass red giant stars reported in this paper with a single CORALIE or FEROS epoch spectra, including the name of the observed star, the astrometric excess noise (AEN) measurements from *Gaia* eDR3, the difference between the CORALIE/FEROS RV and the DR2 RV measurements (Δ RV), the RV error from *Gaia* DR2 (eRV) and the classification number.

Star	Δ RV (km s ⁻¹)	eRV (km s ⁻¹)	AEN (mas)	RUWE	Category
HD2259	1.36	0.50	0.45	2.695	1
HD2132	6.27	1.47	1.90	11.862	1 (Binary)
HD6254	-1.61	0.58	0.50	2.6	1
HD74686	10.23	2.45	3.42	19.337	1
HD83674	-2.99	0.27	0.48	2.651	1
HD8410	9.41	0.53	1.33	9.195	1 (Binary)
HD9525	-5.40	1.04	3.00	6.283	1 (Binary)
HD10537	-8.28	0.15	3.61	5.214	1
HD220864	1.82	0.15	0.63	3.578	1
HD29821	-8.29	0.27	0.53	3.027	1
HD21340	-0.53	0.18	0.50	2.95	1
HD169767	-11.6	0.7	0.907	2.618	1
HD4145	0.90	0.15	0.20	0.993	2
HD5676	4.18	0.43	0.32	2.104	2
HD6030	1.26	1.55	0.29	1.984	2
HD22792	-2.63	0.17	0.17	1.229	2
HD18278	-0.29	0.23	1.04	5.464	2
HD36787	-0.24	1.18	0.70	3.83	2 (Binary)
HD6019	-0.53	0.27	0.65	3.323	2
TYC5464-59-1	-0.22	2.09	0.89	5.437	2
HD10268	-0.22	0.15	0.28	1.719	2
HD193937	-0.18	0.18	0.16	1.354	2
HD93410	0.18	0.17	0.133	1.06	2
HD219263	0.11	0.18	0.32	1.212	3
HD745	0.08	0.18	0.17	1.05	3
HD3303	-0.04	0.17	0.15	0.888	3
HD16665	-0.36	0.17	0.15	1.154	3
HD27956	-0.24	0.12	0.16	1.089	3
HD192232	-0.06	0.13	0.15	0.986	3
HD213986	-0.13	0.16	0.18	0.914	3
HD220096	-0.35	0.17	0.31	0.926	3
HD179120	-0.37	0.13	0.11	0.995	3
HD187562	-0.87	0.25	0.07	0.982	3
HD188476	-0.35	0.14	0.11	0.987	3
HD189365	-0.12	0.14	0.11	0.96	3
HD193407	-0.08	0.15	0.12	1.013	3
HD195189	-0.09	0.15	0.13	0.966	3
HD197790	-0.21	0.14	0.13	1.033	3
HD202704	-0.17	0.18	0.14	1.027	3
HD203086	-0.23	0.15	0.13	1.044	3
HD205588	-0.18	0.17	0.12	1.005	3
HD207920	-0.38	0.16	0.12	0.937	3
HD209154	-0.33	0.15	0.13	0.997	3
HD219026	-0.30	0.14	0.16	1.149	3
HD223700	-0.20	0.14	0.13	1.13	3
HD4737	-0.30	0.15	0.16	1.093	3
HD102888	-0.08	0.15	0.107	0.889	3
HD221214	0.03	0.16	0.118	0.957	3
HD84257	-0.03	0.16	0.121	0.972	3
HD90317	0.01	0.18	0.128	0.991	3

Table A.1. Radial velocity measurements for all stars that are presented in this work.

Star	JD -2450000	RV (km s ⁻¹)	RV Error (km s ⁻¹)	Instrument
HD201013	8650.86	-20.16	0.01	CORALIE
	9538.56	-25.73	0.01	CORALIE
HD204381	8650.82	-20.96	0.01	CORALIE
	9538.57	-20.99	0.01	CORALIE
HD206005	8650.85	-9.75	0.01	CORALIE
	9539.52	-9.26	0.01	CORALIE
HD214941	8650.91	5.07	0.01	CORALIE
	9538.57	1.63	0.01	CORALIE
HD217614	8650.79	-13.93	0.01	CORALIE
	9538.56	-24.69	0.01	CORALIE
CD-324787	8649.47	0.7677	0.0053	CORALIE
	9673.49	0.7348	0.0048	CORALIE
CD-397574	8650.60	6.0176	0.0043	CORALIE
	9673.67	5.9716	0.0039	CORALIE
HD102216	8649.58	17.9042	0.004	CORALIE
	9673.70	17.8746	0.0031	CORALIE
HD102805	8651.54	-11.5754	0.0039	CORALIE
	9673.64	-11.0578	0.0032	CORALIE
HD107045	8650.57	-11.6511	0.0033	CORALIE
	9673.68	-11.6529	0.0032	CORALIE
HD112521	8651.57	7.0568	0.0042	CORALIE
	9673.73	10.7717	0.0033	CORALIE
HD114430	8651.58	-15.8567	0.0045	CORALIE
	9673.72	-15.8535	0.0035	CORALIE
HD116338	8651.59	-30.5275	0.0043	CORALIE
	9673.73	-29.1692	0.0031	CORALIE
HD116845	8650.63	-6.3724	0.0036	CORALIE
	9673.74	-6.3798	0.0038	CORALIE
HD116948	8651.56	-18.5105	0.0039	CORALIE
	9673.75	-18.4976	0.0032	CORALIE
HD119483	8649.55	11.7157	0.011	CORALIE
	9673.76	11.7758	0.003	CORALIE
HD120144	8650.65	-0.6528	0.0031	CORALIE
	9673.76	-0.6394	0.0032	CORALIE
HD122568	8651.61	17.9469	0.0042	CORALIE
	9673.78	17.9291	0.0031	CORALIE
HD124461	8650.67	-40.6677	0.0029	CORALIE
	9673.79	-40.6757	0.0032	CORALIE
HD136350	8649.64	3.7816	0.0048	CORALIE
	9673.81	-6.1007	0.0034	CORALIE
HD139137	8650.69	-39.984	0.0061	CORALIE
	9673.82	-39.0291	0.0068	CORALIE
HD149649	8651.64	7.936	0.005	CORALIE
	9673.82	7.9822	0.0035	CORALIE
HD157527	8649.60	-52.1753	0.0044	CORALIE
	9673.85	-52.4809	0.0034	CORALIE
HD162157	8651.68	-21.0394	0.0042	CORALIE
	9673.84	-21.0381	0.0032	CORALIE
HD162984	8649.62	-9.9796	0.0046	CORALIE
	9673.85	-10.0147	0.0032	CORALIE
HD167768	8650.81	1.6223	0.0053	CORALIE
	9673.89	1.6237	0.0048	CORALIE

Table A.2. Radial velocity measurements for all stars that are presented in this work.

Star	JD -2450000	RV (km s ⁻¹)	RV Error (km s ⁻¹)	Instrument
HD167936	8651.70	-21.1005	0.0065	CORALIE
	9673.86	-37.3306	0.0057	CORALIE
HD168839	8650.89	14.4398	0.0032	CORALIE
	9673.87	14.4181	0.0028	CORALIE
HD170105	8651.66	30.6076	0.0038	CORALIE
	9673.86	31.6746	0.0031	CORALIE
HD171864	8650.70	-17.2808	0.0027	CORALIE
	9673.87	-17.2956	0.0029	CORALIE
HD176771	8649.70	-10.2239	0.006	CORALIE
	9673.88	-10.1944	0.0036	CORALIE
HD191716	8650.80	-7.8355	0.0029	CORALIE
	9673.88	-7.8428	0.0031	CORALIE
HD305357	8650.52	-0.7367	0.0057	CORALIE
	9673.58	3.5397	0.0045	CORALIE
HD71464	8649.50	16.7708	0.0088	CORALIE
	9673.53	39.4804	0.0049	CORALIE
HD85885	8650.55	27.0625	0.0063	CORALIE
	9673.56	26.8646	0.0052	CORALIE
HD96627	8651.47	3.2028	0.0036	CORALIE
	9673.60	3.1933	0.0032	CORALIE
HD99783	8649.60	12.5647	0.005	CORALIE
	9673.61	12.5581	0.0034	CORALIE
HD99891	8651.50	-14.3367	0.004	CORALIE
	9673.62	-14.4727	0.0032	CORALIE

Appendix A: Radial velocity measurements